International Journal of Remote Sensing

ISSN: 0143-1161 (Print) 1366-5901 (Online) Journal homepage: https://www.tandfonline.com/loi/tres20

On the use of the SOS metaheuristic algorithm in hybrid image fusion methods to achieve optimum spectral fidelity

Cigdem Serifoglu Yilmaz, Volkan Yilmaz & Oguz Güngör

To cite this article: Cigdem Serifoglu Yilmaz, Volkan Yilmaz & Oguz Güngör (2020) On the use of the SOS metaheuristic algorithm in hybrid image fusion methods to achieve optimum spectral fidelity, International Journal of Remote Sensing, 41:10, 3993-4021, DOI: 10.1080/01431161.2019.1711244

To link to this article: https://doi.org/10.1080/01431161.2019.1711244

INTERNATIONAL JOURNAL OF REMOTE SENSING
2020, VOL. 41, NO. 10, 3993–4021
https://doi.org/10.1080/01431161.2019.1711244

Taylor & Francis
Taylor & Francis Group

On the use of the SOS metaheuristic algorithm in hybrid image fusion methods to achieve optimum spectral fidelity

Cigdem Serifoglu Yilmaz[a], Volkan Yilmaz[b] and Oguz Güngör[a]

[a]Department of Geomatics, Karadeniz Technical University, Trabzon, Turkey; [b]Department of Geomatics, Artvin Coruh University, Artvin, Turkey

ABSTRACT

Image fusion aims to spatially enhance a low-resolution multispectral (MS) image by utilizing a high-resolution panchromatic (Pan) band. Various image fusion methodologies have been proposed with the aim to improve the spatial detail quality without deteriorating the colour content of the input MS image. Previous studies revealed the fact that there is no such thing as 'the best image fusion method' since all fusion methods cause either spectral distortion or spatial detail loss to some extent, which motivates the researchers to develop more advanced methods to keep the colour content while increasing the spatial detail quality. This study proposed to use the Symbiotic Organisms Search (SOS) metaheuristic algorithm in hybrid image fusion methods to achieve the optimum colour quality in the fused images. The SOS algorithm was used in two hybrid fusion approaches, one including the Intensity-Hue-Saturation (IHS) and Discrete Wavelet Transform (DWT) methods and the other one including the IHS and Discrete Wavelet Frame Transform (DWFT) methods. The results of the proposed methods were qualitatively and quantitatively compared in three test sites against those of eighteen widely-used image fusion methods. It was concluded that the proposed methods led to superior colour quality with both singlesensor and multisensor input images, regardless of the spatial resolution difference between the input images. The proposed methods were also found to be very successful in sharpening the images, despite the fact that their main purpose was to keep the colour content as much as possible.

ARTICLE HISTORY
Received 3 July 2019
Accepted 6 November 2019

1. Introduction

Image fusion integrates the spectral characteristics of a low-resolution multispectral (MS) image and spatial features of a high-resolution panchromatic (Pan) band, producing an image of superior colour and spatial detail quality (Yilmaz and Gungor 2016a). In parallel to the developments in the sensor technology of the satellites and manned/unmanned aerial vehicles, image fusion has been one of the hottest topics of image processing since the 1980s. The main objective of image fusion is to increase the useful information content of an image to improve the performance of further image processing applications such as feature extraction and segmentation (Li, Manjunath, and Mitra 1995).

CONTACT Volkan Yilmaz volkanyilmaz.jdz@gmail.com Department of Geomatics, Artvin Coruh University, Artvin, 08100, Turkey

The success of image fusion process depends on some factors: (1) It is rather easier to fuse the MS and Pan bands that are acquired from the same sensor, since they cover the same wavelength interval in the electromagnetic spectrum. However, when using multisensor input images, wavelength differences may lead to significant colour distortions even if the images are acquired on the same date. (2) The spatial resolution difference between the input images is another factor that should be considered before fusing the images. The greater spatial resolution difference between the input images, the more challenging fusion process (Yilmaz and Gungor 2016a). (3) The input images should be co-registered to the same projection; otherwise, artificial colours or features will occur on the fused images (Pohl and Van Genderen 1998). (4) If needed, prior to fusion, atmospheric and radiometric correction should be applied on the input images to avoid any colour distortions. (5) The operator's fusion experience is also another factor that plays an important role in the success of the fusion process (Zhang 2004).A wide variety of image fusion methods have been proposed in the literature so far. A very comprehensive and helpful literature review on the image fusion methods was provided by Pohl and Van Genderen (1998), 2016). The analysts who are in the need to fuse images should keep in mind that there is no such thing as 'the best image fusion method' (Pohl and van Genderen 2016). The reason for this is that all fusion methods are expected to distort the colour characteristics of the input MS image and to deteriorate the spatial details of the input Pan band to some extent. Hence, any method ensuring the optimum spatial and spectral quality is considered successful.

Image fusion methods can be classified into four categories as the component substitution (CS) based, multiresolution analysis (MRA) based, colour based (CB) and hybrid methods. The CS based methods transform the input MS image into another space where the spatial characteristics are separated from the colour content in different components. Then, the component containing the spatial content is substituted with the input Pan band. A reverse transformation to the original space results in the fused image (Ghassemian 2016). The Intensity-Hue-Saturation (IHS) (Haydn et al. 1982), Brovey (BRV) (Hallada and Cox 1983), Principal Component Analysis (PCA) (Chavez and Kwarteng 1989) and Gram-Schmidt (GS) (Laben and Brower 2000) are among the most famous members of this fusion family. According to Ghassemian (2016), the MRA methods, so-called multi-scale decomposition based methods, include three main steps: (1) The input images are decomposed into several scales through some transforms such as wavelet, curvelet, contourlet etc. (2) The fusion takes place at each level of decomposition. (3) An inverse transform is applied to obtain the fused bands. The Additive Wavelet Luminance Proportional (AWLP) (Otazu et al. 2005), Generalized Laplacian Pyramid (GLP) with Modulation Transfer Function (MTF) matched filter (MTF-GLP) (Aiazzi et al. 2006), MTF-GLP with High-Pass Modulation (MTF-GLP-HPM) (Vivone et al. 2014), GLP with MTF-matched filter and Context-Based Decision (CBD) injection scheme (MTF-GLP-CBD) (Alparone et al. 2007) methods are some of the most widely-used MRA methods. The CB methods aim to keep the statistical characteristics of the MS bands after fusion. The most commonly-used CB methods include the Local Mean Matching (LMM) (de Béthune, Muller, and Binard 1997), Local Mean Variance Matching (LMVM) (de Béthune, Muller, and Binard 1997), Smoothing Filter-based Intensity Modulation (SFIM) (Liu 2000) and Nearest Neighbour Diffuse (NND) (Sun, Chen, and Messinger 2014). The hybrid fusion methods combine the superiorities

of the methods from several categories to keep the colour content while transferring the spatial details.

1.1. Motivation

El-Samie, Hadhoud, and El-Khamy (2012) indicated that it is possible to combine the IHS and MRA based methods Discrete Wavelet Transform (DWT) and Discrete Wavelet Frame Transform (DWFT). Such a hybrid fusion approach allows for making full use of both IHS method's spatial detail transfer advantage and wavelet decomposition's colour preservation advantage. On the other hand, the performance of the IHS method depends heavily on the procedure used to compute the intensity component to be swapped with the input Pan band, which attaches importance on finding the optimum band weights to achieve the optimum intensity component. The most commonly-used IHS transformation procedures consider equal band weights to compute the intensity component. However, this approach is not efficient for image fusion because, in reality, each input MS band has a different effect on the intensity component and, of course, on the fusion result. Hence, more effective strategies should be developed to optimize the intensity component used by the IHS fusion method. To this aim, this study, for the first time in the literature, proposed a hybrid image fusion framework that uses the Symbiotic Organisms Search (SOS) metaheuristic algorithm (Cheng and Prayogo 2014) to calculate the optimum intensity component to be used within the IHS transform. The second step of the framework includes the wavelet decomposition of the input bands. A detailed literature review revealed the fact that very few studies focused on using metaheuristic algorithms to obtain the optimum fusion results. The Genetic Algorithm (GA) (Holland 1975), the first metaheuristic algorithm used for optimization purposes, was previously used to improve the performance of the Generalized IHS (Garzelli and Nencini 2006a), ATWT (Garzelli and Nencini 2006b), IHS (Masoudi and Kabiri 2014; Niazi, Zade, and Zadeh 2016) and Synthetic Variable Ratio (Yilmaz, Serifoglu Yilmaz, and Gungor 2019) methods. However, to the best of our knowledge, the SOS algorithm has never been used to improve the performance of such a hybrid approach that includes both the IHS and DWT/DWFT methods. This study will fill this gap in the literature.

2. IHS, DWT and DWFT methods

2.1. IHS method

The IHS is one of the most widely-used conventional image fusion methods. The very first step of this method is to upsample the input MS bands to the size of the input Pan band. The upsampled bands are then transformed into the intensity, hue and saturation components. The hue is related to the pure colours of the objects and is represented by an angle. The saturation shows to what degree a pure colour is diluted by white colour. The intensity, which is measurable and interpretable, is the most useful descriptor of monochromatic images (El-Samie, Hadhoud, and El-Khamy 2012). Transformation from the RGB to IHS space stores the colour features in the hue and saturation components and most of the spatial detail content in the intensity component. After the IHS transform, the histogram of the Pan band is matched to that of the intensity component to reduce the colour distortion after

fusion. As a final step, an inverse IHS transform is applied using the hue, saturation and histogram-matched Pan band to obtain the fused bands in the RGB space (Haydn et al. 1982). The conventional IHS fusion method can handle MS images with three MS bands, which is the biggest limitation of this method. Siddiqui (2003) introduced a modified IHS (MIHS) method that is able to cope with images with more than three MS bands.

Various transformation procedures have been introduced in the literature to transform the MS bands from RGB into IHS space, and vice versa. This study used one of the most widely-used transformation models given as (Elkaffas et al. 2006; Gonzalez and Woods 2007; El-Samie, Hadhoud, and El-Khamy 2012);

$$\begin{pmatrix} \mathrm{DN_I} \\ V_1 \\ V_2 \end{pmatrix} = \begin{pmatrix} \frac{1}{3} & \frac{1}{3} & \frac{1}{3} \\ \frac{-\sqrt{2}}{6} & \frac{-\sqrt{2}}{6} & \frac{\sqrt{2}}{6} \\ \frac{1}{\sqrt{2}} & \frac{-1}{\sqrt{2}} & 0 \end{pmatrix} \begin{pmatrix} \mathrm{DN_R} \\ \mathrm{DN_G} \\ \mathrm{DN_B} \end{pmatrix} \tag{1}$$

$$H = \tan^{-1}\left(\frac{V_2}{V_1}\right) \tag{2}$$

$$S = \sqrt{V_1^2 + V_2^2} \tag{3}$$

Transformation from IHS to RGB space is given as;

$$\begin{pmatrix} \mathrm{DN_R} \\ \mathrm{DN_G} \\ \mathrm{DN_B} \end{pmatrix} = \begin{pmatrix} 1 & \frac{-1}{\sqrt{2}} & \frac{1}{\sqrt{2}} \\ 1 & \frac{-1}{\sqrt{2}} & \frac{-1}{\sqrt{2}} \\ 1 & \sqrt{2} & 0 \end{pmatrix} \begin{pmatrix} \mathrm{DN_{Pan}} \\ V_1 \\ V_2 \end{pmatrix} \tag{4}$$

where, $\mathrm{DN_R}$, $\mathrm{DN_G}$, $\mathrm{DN_B}$, $\mathrm{DN_I}$ and $\mathrm{DN_{Pan}}$ refer to a digital number (i.e. grey value) in the red band, green band, blue band, intensity component and input Pan band, respectively. V_1 and V_2 are also constants.

2.2. DWT and DWFT methods

The wavelet transform decomposes an image into multiple wavelet planes based on local frequency content, producing images with coarser resolutions. Various wavelet transform-based fusion approaches have been used in the literature. Li, Kwok, and Wang (2002) presented a general four-step framework for wavelet-based fusion approaches as: (1) The input images are registered and resampled to the same size. (2) The images are decomposed to the same resolution using the DWT. (3) Corresponding wavelet coefficients are combined with respect to a fusion rule. (4) An inverse wavelet transform is applied to produce the fused image.

The DWT fusion method used in this study is applied as follows. As a first step, the input Pan band is decomposed into wavelet planes using the DWT until the spatial resolution of the input MS image is reached. Note that each decomposition generates four wavelet planes with half resolution. The first wavelet plane includes the approximation coefficients that are related to the colour characteristics of the Pan band. The other three wavelet planes comprise the high-frequency details (i.e. spatial details) in horizontal, vertical and diagonal directions. Once the wavelet decompositions are done, all input MS bands are replaced by

the approximation coefficients at the coarsest resolution one by one and the whole procedure is reversed back by applying an inverse DWT to obtain the fused bands.

The main difference between the DWT and DWFT methods is that the DWT method uses decimation and the DWFT does not (El-Samie, Hadhoud, and El-Khamy 2012). The DWFT uses the à trous algorithm to decompose an image into additive components, each being a sub-band of the image. This procedure enables the isolation of different frequency components into different planes without being have to apply downsampling as in the DWT. The differences between two successive approximations are used as the wavelet detail planes. The first step of the DWFT method is to decompose the input MS and Pan bands using the DWFT. The high-frequency detail components obtained from the Pan band are then combined with the lowest-frequency approximation component obtained from each MS band. An inverse DWFT is applied to produce the fused bands (Li, Kwok, and Wang 2002; El-Samie, Hadhoud, and El-Khamy 2012). Interested readers are referred to the works by Gonzalez and Woods (2007) and El-Samie, Hadhoud, and El-Khamy (2012) for further details about wavelet-based image fusion.

2.3. Hybrid fusion approach based on the IHS and DWT/DWFT

El-Samie, Hadhoud, and El-Khamy (2012) indicated that it is possible to combine the IHS with the DWT and DWFT methods to produce fused images with superior colour and spatial fidelity. The steps for such fusion was given as: (1) The input MS and Pan bands are co-registered. (2) The MS image is transformed into the IHS space. (3) The histogram of the input Pan band is matched to that of the intensity component to preserve the colour balance after fusion. (4) A DWT or DWFT is applied on both the histogram-matched Pan band and intensity component. (5) The approximation component obtained from the intensity component is substituted by its average with the approximation component obtained from the histogram-matched Pan band. (6) A new intensity component is produced by applying an inverse DWT or DWFT on the approximation component and high-frequency detail components. (7) An inverse IHS transform is applied on the new intensity, hue and saturation components to produce the fused image in the RGB space (El-Samie, Hadhoud, and El-Khamy 2012). Such a hybrid fusion approach based on the IHS and wavelet decomposition was also used by Zhang and Hong (2005).

3. SOS algorithm

The SOS algorithm, proposed by Cheng and Prayogo (2014), searches for the optimum solutions for many tough optimization problems, even if the search space is very large and complex. It is based on the symbiotic relationships between living organisms. The SOS algorithm starts by randomly generating a group of 'organisms', each including the parameters that are candidate for optimal solution. All organisms form the 'ecosystem'. Next generations of the ecosystem are formed through the imitation of the symbiotic relationship between two organisms. The mutualism, commensalism and parasitism are the most common symbiotic relationships exist in nature (Cheng and Prayogo 2014).

The mutualism refers to a symbiotic relationship that is beneficial for both of the organisms of different species involved in the association. According to this operator,

candidate solutions are modified by calculating the difference between the optimal solution and the mean of two organisms. Let $\boldsymbol{X}_i$ be an organism that is matched to the i^{th} member of the ecosystem. Another organism $\boldsymbol{X}_j$ is randomly selected from the ecosystem. Both organisms 'work together' in a mutualistic relationship to increase the mutual survival advantage in the ecosystem. New candidate solutions ($\boldsymbol{X}_{i-\text{new}}$, $\boldsymbol{X}_{j-\text{new}}$) for these organisms are calculated as (Cheng and Prayogo 2014);

$$\boldsymbol{X}_{i-\text{new}} = \boldsymbol{X}_i + \boldsymbol{r}(0,1) \times (\boldsymbol{X}_{\text{best}} - \boldsymbol{M} \times \boldsymbol{B}_1) \tag{5}$$

$$\boldsymbol{X}_{j-\text{new}} = \boldsymbol{X}_j + \boldsymbol{r}(0,1) \times (\boldsymbol{X}_{\text{best}} - \boldsymbol{M} \times \boldsymbol{B}_2) \tag{6}$$

$$\boldsymbol{M} = \frac{\boldsymbol{X}_i + \boldsymbol{X}_j}{2} \tag{7}$$

where, $\boldsymbol{M}$ is the mutual vector, $\boldsymbol{X}_{\text{best}}$ is the ecosystem member (organism) with the best fitness value, $\boldsymbol{r}(0,1)$ is a vector comprising random numbers between 0 and 1. B_1 and B_2 refer to the benefit factors that specify to what degree each organism benefits from this relationship. B_1 and B_2 get values of 1 or 2.

The commensalism, which originated from the Latin word 'commensalis' (derived from the words 'com' (together) and 'mensa' (table), meaning 'eating at the same table'), is a symbiotic relationship between two organisms where only one benefits without harming the other one. The commensalism operator calculates the difference between solutions to modify a solution. Let $\boldsymbol{X}_j$ be an organism that is randomly selected from the ecosystem. The commensal symbiosis between $\boldsymbol{X}_i$ and $\boldsymbol{X}_j$ is considered to obtain the new candidate solution for $\boldsymbol{X}_i$ ($\boldsymbol{X}_{i-\text{new}}$). The organism $\boldsymbol{X}_i$ is updated only when the computed fitness value is better than the pre-interaction fitness value (Cheng and Prayogo 2014).

$$\boldsymbol{X}_{i-\text{new}} = \boldsymbol{X}_i + \boldsymbol{r}(-1,1) \times \left(\boldsymbol{X}_{\text{best}} - \boldsymbol{X}_j\right) \tag{8}$$

where, $\boldsymbol{r}(-1,1)$ is a random vector of numbers ranging between −1 and 1, and $\boldsymbol{X}_{\text{best}}$ defines the organism with the best fitness value.

The parasitism refers to a symbiotic relationship between two organisms in which one, the parasite, gains benefits and the other one, the host, is harmed. The parasitism operator, which ensures the mutation in the ecosystem, modifies the solution by making random changes in the organisms. After the application of the mutation operator, any organism that is found to be harmed perishes whereas the organisms that benefitted are evolved to a fitter organism. The best organism in the ecosystem is updated once the mutualism, commensalism and parasitism operators are applied to each organism (Cheng and Prayogo 2014). The SOS algorithm iterates until a stopping criterion is satisfied or maximum iteration number is reached (Tran, Cheng, and Prayogo 2016).

4. Material and methodology

4.1. Test sites and data used

This study was conducted in three test sites in the city of Trabzon, which is located on the northeast coast of Turkey. Plenty of attention was paid to define the test sites that

included many types of land cover to ensure a comprehensive performance comparison between the proposed approaches and other image fusion methods used.

The first test site, which was a mixture of urban and rural area, was acquired in 2012 by the WorldView-2 satellite that collects the electromagnetic energy in eight MS bands (i.e. coastal, blue, green, yellow, red, red edge, near-infrared 1 and near-infrared 2) with 2 m spatial resolution and a Pan band with 0.5 m spatial resolution.

The second test site, which had similar land cover features as the first site, was acquired in 2003 by the IKONOS satellite that offers four MS bands (i.e. blue, green, red and near-infrared) with 4 m spatial resolution. The Pan band for the second site was produced by averaging the MS bands (i.e. blue, green, red and near-infrared) of a QuickBird pansharpened image, which was acquired in 2005 and had a spatial resolution of 60 cm. Despite the two-year difference in the acquisition dates of the input images of this site, there were no land cover changes within this period that would have led to significant fusion problems.

The third test site, which was a highland area including a mixture of buildings and vegetation, was acquired by the WorldView-2 satellite in 2013. The Pan band used for this site was generated by averaging an orthophoto, which was produced by processing the aerial photos captured in 2013 by a 10-MP RICOH GR DIGITAL IV digital camera mounted on a Gatewing X100 unmanned aerial vehicle (UAV). With a 40-min flight, 256 aerial photos (8 bits) were captured from an altitude of 185 m. The Agisoft Photoscan Professional software was used to produce the orthophoto. Since the WorldView-2 imagery had a radiometric resolution of 11 bits, the orthophoto was scaled to 11 bits to match the dynamic ranges. The input MS image of this site was co-registered with respect to the Pan band so that both images were aligned to be fused properly. The input Pan band of the third site had a spatial resolution of 20 cm and the input MS image had a spatial resolution of 2 m, which made the fusion process more challenging in this site, compared to the other sites. Figure 1 shows the test sites.

4.2. Proposed SOS-based hybrid image fusion frameworks

The biggest problem with the CS-based image fusion methods is that they tend to distort the colour content of the input MS image (Ghassemian 2016), due to the procedures used to generate the intensity component. The performance of the IHS fusion method depends on the IHS transform model used. Despite the fact that different transformation models with different complexities have been proposed so far, all of them produce similar values for the hue and saturation components. However, the models differ in the procedure utilized to compute the intensity component (Nunez et al. 1999). As seen in Equation 1, weights for the red, green and blue bands are considered equal, which is the main reason for the colour distortion caused by the IHS method. A similar problem can be observed in the BRV method, which uses equal band weights to construct the intensity component. Munechika et al. (1993) and Zhang (1999) focused on using regression analysis to estimate more efficient band weights to minimize the colour distortion in CS-based methods.

The proposed fusion frameworks follow these steps:

(1) The input MS image is upsampled to the size of the input Pan band.
(2) The ecosystem is generated randomly. Each organism is a vector comprising numbers that are randomly generated between 0 and 1. The experiments revealed

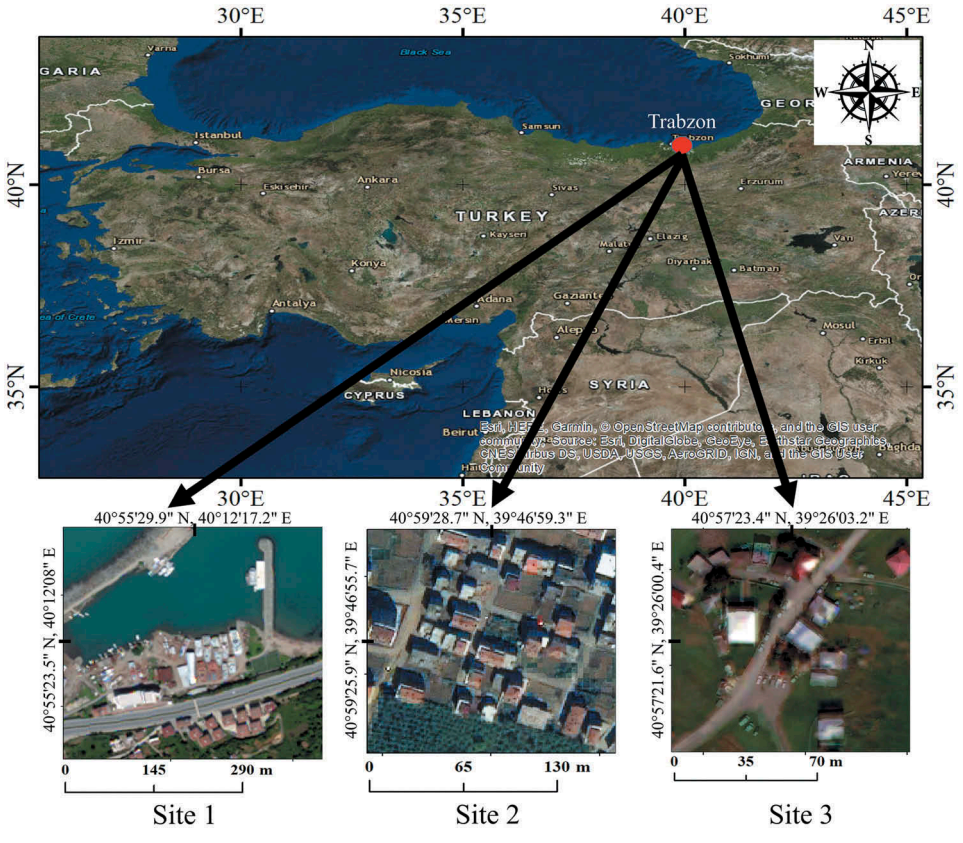

Figure 1. Test sites.

the fact that the SOS algorithm converged very fast and that there was no need for greater ecosystem sizes. Hence, the ecosystem sizes of 100, 100 and 200 were considered adequate for the sites 1, 2 and 3, respectively.

(3) The IHS-DWT or IHS-DWFT methods are applied as the objective functions of the SOS algorithm. The dependent and independent variables of the objective functions are the band weights and input bands, respectively. In this step, the IHS method is applied by using the Equations 1, 2 and 3 in order to transform the MS bands from the RGB to IHS space. Instead of using equal band weights for all MS bands (as in the Equation 1), the proposed approach uses the members of each organism as the band weights and calculates an intensity component as the weighted average of the input MS bands. Once the intensity component is produced, the histogram of the input Pan band is matched to that of the intensity component to keep the colour content as much as possible. A DWT or DWFT is applied on both the histogram-matched Pan band and the intensity component. The approximation component obtained from the intensity component is replaced by its average with the approximation component obtained from the histogram-matched Pan band. An inverse DWT or DWFT is then applied on the approximation component and high-frequency components to produce a new intensity

component. The fused image is produced by applying an inverse IHS transform (Equation 4) on the new intensity, hue and saturation components.

(4) The fitness function is computed for each fused image. The Erreur Relative Globale Adimensionnelle de Synthése (ERGAS) (Wald 2000) metric was used as the fitness function of the SOS algorithm. The ERGAS metric was calculated between the input MS bands and corresponding fused bands. The reason for using the ERGAS metric as the fitness function was that this metric has been proven to be one of the best indicators of colour quality between images. Since the optimum ERGAS value is 0, the algorithm tried to minimize the ERGAS value in each SOS iteration.

(5) If the stopping criterion is not satisfied, the SOS algorithm employs the mutualism (using the Equations 5, 6 and 7), commensalism (using the Equation 8) and parasitism operators to generate a new ecosystem with new organisms. The difference between the best fitness (ERGAS) value and global minimum ERGAS value within each iteration was set as the stopping criterion. In light of this, in this study, a difference value below 1E-03 was selected as the stopping criterion of the SOS algorithm. Theoretically, it was not possible to obtain an ERGAS value of 0 (otherwise, the fused image would be identical to the input MS image); hence, a maximum iteration number of 300 was selected for all test sites to terminate the iterations.

(6) The SOS iterations continue with new ecosystems until the stopping criterion is satisfied or the maximum number of iterations is reached. Since all input MS images had more than three MS bands, the proposed frameworks were applied using trilateral combinations of the MS bands. It should also be noted that the proposed frameworks were encoded in MATLAB environment. The optimum band weights of 0.12, 0.14, 0.21, 0.28, 0.06, 0.08, 0.04 and 0.05; 0.24, 0.26, 0.34 and 0.18; and 0.10, 0.16, 0.17, 0.31, 0.08, 0.05, 0.06 and 0.06 were achieved for the input MS images of the sites 1, 2 and 3, respectively. The flowchart of the proposed SOS-based IHS-DWT (SIHS-DWT) and SOS-based IHS-DWFT (SIHS-DWFT) frameworks are shown in Figure 2.

4.3. Image fusion methods used

This subsection provides brief theoretical information about the methodologies of the image fusion methods compared against the proposed fusion frameworks. This study used the CS-based methods IHS, BRV, PCA, GS, Ehlers (Ehl), BDSD and HCS. The BRV method normalizes the MS image by dividing it with an intensity component obtained by summing all MS bands and multiplies the result by the Pan band to produce the fused bands (Hallada and Cox 1983). The PCA method transforms the MS image into a new space where most of the spatial detail content is stored in the first principal component (PC1) and the spectral information is mapped into other components. Then, the PC1 is substituted by the Pan band, whose mean and variance information is matched to those of the PC1. Finally, an inverse PCA transform is applied to compute the fused image (Chavez and Kwarteng 1989). The GS, which is another statistical method, is a generalized version of the PCA method. As a first step, the GS method interpolates all MS bands to the scale of the input Pan band. All input bands are then converted to vectors. Afterwards, a low-resolution Pan band is simulated using the MS vectors. Then, the MS and simulated Pan vectors are combined, simulated Pan vector being the first. A GS transform is applied on the combined data and the first GS

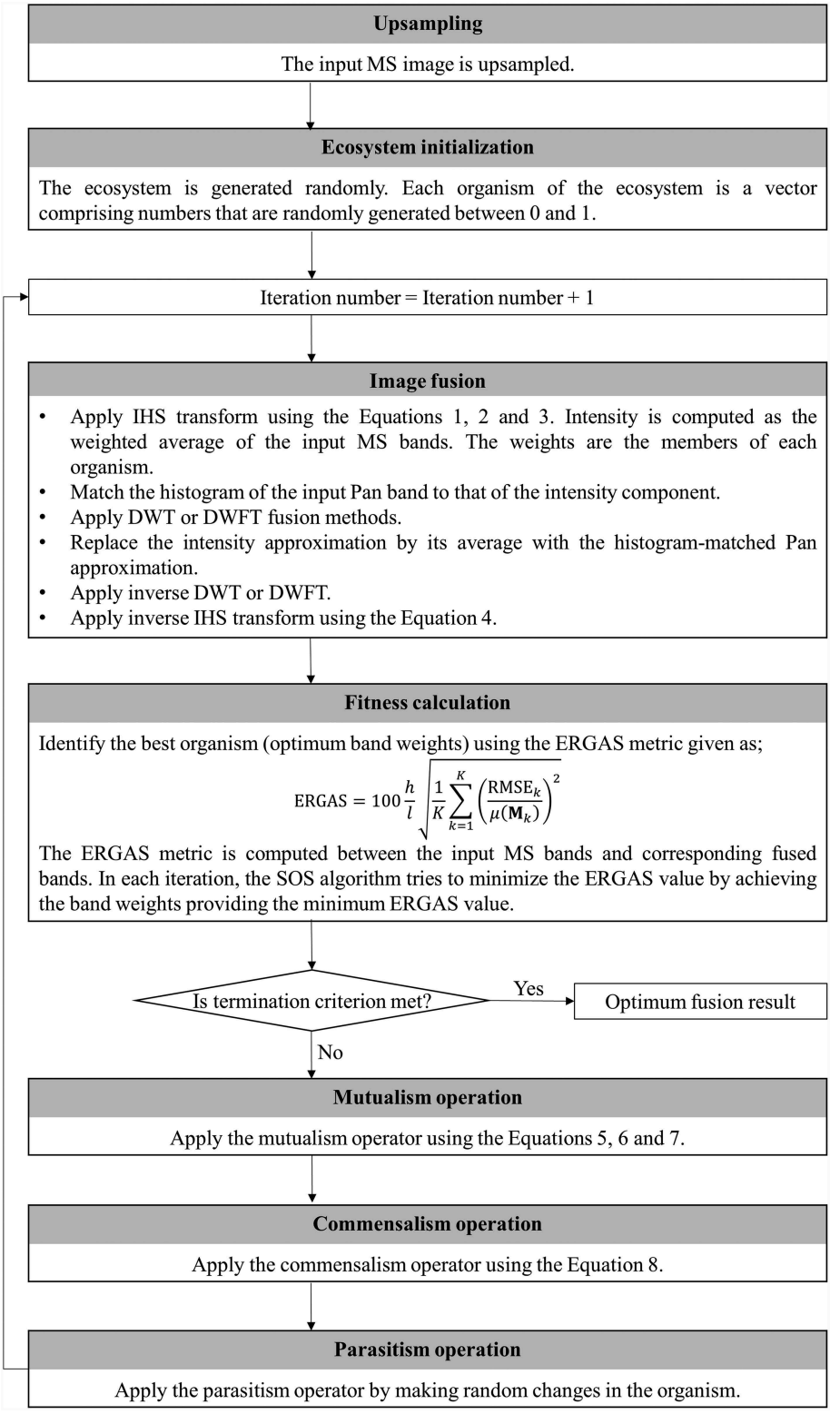

Figure 2. Flowchart of the proposed fusion methods.

component is replaced by the input Pan vector. A reverse GS transform results in the fused image (Laben and Brower 2000). The Ehl, one of the most widely-used fusion methods, utilizes both the IHS and Fast Fourier Transforms (FFT). As a first step, an IHS transform is applied on the input MS image and an FFT is applied on both the input Pan band and intensity component obtained from the IHS transformation. The intensity spectrum is filtered with a low-pass filter and the Pan spectrum is filtered with a high-pass filter. An intermediary intensity component is generated by adding the filtered spectrums. The fused image is obtained through an inverse IHS transformation applied on the new intensity, hue and saturation components (Ehlers 2004; Klonus and Ehlers 2007). The Band Dependent Spatial Detail (BDSD) method, proposed by Garzelli, Nencini, and Capobianco (2008), spatially enhances a degraded version of the input MS image from a degraded version of the Pan band, minimizing the squared error between the MS bands and fused bands. The coefficients of the weighted summation of the MS bands are defined band dependent, calculating a different optimal detail image for each MS band (Garzelli, Nencini, and Capobianco 2008; Imani 2018). The Hyperspherical Colour Space (HCS) method transforms the input MS image from the native colour space (i.e. RGB) to HCS colour space, which consists of an intensity component and $N-1$ angular components, N being the number of input MS bands. An adjusted intensity is then produced by dividing the Pan band by a smoothed version of the Pan band and multiplying the result by the intensity component. The adjusted intensity is replaced by the intensity component and an inverse HCS transformation results in the fused image (Padwick et al. 2010).

The MRA-based fusion methods used in this study were the AWLP, MTF-GLP, MTF-GLP-HPM and MTF-GLP-CBD. The AWLP method keeps the proportion between pixel vectors by proportionally injecting the high-frequency details extracted with the à trous wavelet transformation into the MS bands (Otazu et al. 2005). The MTF-GLP fusion method injects the spatial details of the input Pan band considering a constraint of thoroughly retaining the spectral characteristics of the coarser-resolution input MS image. A MTF of the input MS image is used to form a GLP reduction filter. The Interband Structure Model (IBSM), which is computed at the coarser scale, where the input MS and Pan bands are available, is extended to a finer scale (Aiazzi et al. 2006). The MTF-GLP-HPM method uses the MTF before downsampling and employs the HPM injection procedure (Vivone et al. 2014). The MTF-GLP-CBD method employs a decision model based on locally thresholding Pearson's correlation coefficient (r) between each resampled MS band and the low-pass approximation of the input Pan band (Alparone et al. 2007).

This study used the CB methods LMM, LMVM, SFIM and NND. The LMM method, as the name implies, matches the local mean values of the Pan image with those of the MS bands by using normalization functions at a local scale (de Béthune, Muller, and Binard 1997). The LMVM method matches the local mean and variance values between the input images (de Béthune, Muller, and Binard 1997). The SFIM method, as a first step, applies a low-pass filter on the Pan band. Then, each MS band is multiplied by the Pan band and the result is divided by the low-pass filtered Pan band (Liu 2000). The NND method considers each pixel spectrum in the fused image as a weighted linear mixture of the spectra of the neighbouring superpixels (Sun, Chen, and Messinger 2014).

5. Results and discussion

The spectral fidelities of all fusion results were evaluated qualitatively and quantitatively. The performances of the proposed SIHS-DWT and SIHS-DWFT frameworks were compared against those of widely-used image fusion methods BRV, MIHS, HCS, EhI, PCA, GS, BDSD, LMM, LMVM, NND, DWT, DWFT, MTF-GLP, MTF-GLP-CBD, MTF-GLP-HPM, SFIM and AWLP. According to Wald's first property (Wald, Ranchin, and Mangolini 1997), a fused image that is downsampled to the size of the input MS image should be as identical as possible to the MS image. Hence, to evaluate the spectral quality of the fused images, the Root Mean Square Error (RMSE) (Wald and Ranchin 2002), Relative Average Spectral Error (RASE) (Ranchin and Wald 2000), ERGAS, Information Content Weighted Structural Similarity (IW-SSIM) (Wang and Li 2011), Universal Image Quality Index (UIQI) (Wang and Bovik 2002), Multi-Scale Structural Similarity (MS-SSIM) (Wang, Simoncelli, and Bovik 2003), Structural Similarity Index (SSIM) (Wang et al. 2004), Spectral Information Divergence (SID) (Strait, Rahmani, and Markurjev 2008), Spectral Angular Mapper (SAM) (Alparone et al. 2006, 2007) and r (Zeng et al. 2010) metrics were computed between the input MS bands and fused bands that were downsampled to the size of the input MS image. The SSIM, IW-SSIM, r and Spatial Correlation Coefficient (r_s) (Zhou, Civco, and Silander 1998) metrics were also computed between the input Pan band and fused bands in order to evaluate the spatial quality of the fused images. Table 1 shows the mathematical theories of the quality metrics used in this study. Note that the optimum

Table 1. Mathematical theories of the quality metrics used.

Metric	Formula
RMSE	$\mathrm{RMSE} = \sqrt{\frac{1}{n}\sum_{i=1}^{n}\left(\mathbf{M}(k)_i - \mathbf{P}(k)_i\right)^2}$
RASE (%)	$\mathrm{RASE} = \frac{100}{M}\sqrt{\frac{1}{K}\sum_{k=1}^{K}\left(\mathrm{RMSE}(\mathbf{M}_k)\right)^2}$
ERGAS	$\mathrm{ERGAS} = 100\frac{h}{l}\sqrt{\frac{1}{K}\sum_{k=1}^{K}\left(\frac{\mathrm{RMSE}_k}{\mu(\mathbf{M}_k)}\right)^2}$
IW-SSIM	$\mathrm{IW}-\mathrm{SSIM}_j = \frac{\sum_i w_{j,i}c\left(x_{j,i},y_{j,i}\right)s\left(x_{j,i},y_{j,i}\right)}{\sum^{w_{j,i}}}\mathrm{IW}-\mathrm{SSIM} = \prod^{\left(\mathrm{IW}-\mathrm{SSIM}_j\right)^{\beta_j}}$
UIQI	$\mathrm{UIQI} = \frac{4\mu_x\mu_y\sigma_{x,y}}{\left(\mu_x^2+\mu_y^2\right)\left(\sigma_x^2+\sigma_y^2\right)}$
MS-SSIM	$\mathrm{MS}-\mathrm{SSIM} = \left[l_T(x,y)\right]^{\propto_T}\times\prod_{j=1}^{T}\left[c_j(x,y)\right]^{\beta_j}\left[s_j(x,y)\right]^{\gamma_j}$
SSIM	$\mathrm{SSIM} = \frac{\left(2\mu_x\mu_y+C_1\right)\left(2\sigma_{x,y}+C_2\right)}{\left(\mu_x^2+\mu_y^2+C_1\right)\left(\sigma_x^2+\sigma_y^2+C_2\right)}$
SID	$\mathrm{SID} = D(x \parallel y) + D(y \parallel x)D(x \parallel y) = \sum^{p_i}\ln\left(\frac{p_i}{q_i}\right)D(y \parallel x) = \sum^{q_i}\ln\left(\frac{q_i}{p_i}\right)p_j = \frac{x_j}{\sum_{i=1}^{K}x_i}q_j = \frac{y_j}{\sum_{i=1}^{K}y_i}$
SAM	$\mathrm{SAM} \triangleq \arccos\left(\frac{\langle x,y\rangle}{\|x\|_2\cdot\|y\|_2}\right)$
r	$r = \frac{\sum_{m,n}\left(\mathbf{M}_{m,n}-\mu(\mathbf{M})\right)\left(\mathbf{P}_{m,n}-\mu(\mathbf{P})\right)}{\sqrt{\left(\sum_{m,n}\left(\mathbf{M}_{m,n}-\mu(\mathbf{M})\right)^2\left(\sum_{m,n}\left(\mathbf{P}_{m,n}-\mu(\mathbf{P})\right)^2\right)}}$
r_s	This metric calculates the r between the Laplacian filtered-fused bands and input Pan band.

where, $\mathbf{M}$ is the input MS image, $\mathbf{P}$ is the fused image, n is the total number of pixels, h is the spatial resolution of the input Pan image, l is the spatial resolution of the input MS image, K is the total number of bands, M is the mean radiance, μ refers to mean, x is the MS pixel vector, y is the fused pixel vector, $\cdot$ refers to dot product, σ refers to variance, w is the information content weight, C_1 and C_2 are constants calculated as $C_1 = (Y_1L)^2$ and $C_2 = (Y_2L)^2$, Y is a small constant, L is the dynamic range of the pixel values, and $\propto_T$, β_j and γ_j are used to adjust the relative importance of different components.

value for the RMSE, RASE, ERGAS, SID and SAM metrics is 0, whereas the optimum value for the IW-SSIM, UIQI, MS-SSIM, SSIM and *r* metrics is 1.

5.1. Qualitative evaluation

Qualitative evaluation, which provides a general overview about the performance of the fusion method used, aims to visually interpret the fused images to see whether the fusion method managed to keep the colour content of the input MS image. Figures 3–5 show the fusion results of the sites 1, 2 and 3, respectively. All images in these figures are displayed in true colour (RGB) band combination. Note that all fused images are displayed without any contrast stretch to ensure a fair comparison among the fusion results. It can be inferred from Figures 3–5 that all fusion methods made changes on the colour characteristics to some extent, which was expected.

As seen in Figure 3, the BRV, MIHS, PCA, GS, NND and DWFT methods caused significant changes in the global colour characteristics of the site 1. These methods caused colour distortions on the vegetation, road and water land classes. On the other hand, the HCS, Ehl, LMM, LMVM, DWT, SFIM, AWLP, SIHS-DWT and SIHS-DWFT methods resulted in more realistic colours in this site. Figure 4 shows that, in the site 2, the BRV, MIHS, HCS, Ehl, NND and DWFT methods caused a greater amount of global colour distortion, compared to the other methods used. The PCA, GS, BDSD, LMVM, DWT, SFIM, SIHS-DWT and SIHS-DWFT methods presented a better performance in terms of keeping the global colour content in the site 2. Another interesting conclusion drawn from the fusion results of the site 2 is that the NND method caused drastic changes in the colours of the shadowy areas. As seen in Figure 5, the MIHS, GS, NND, DWFT, MTF-GLP-HPM and SFIM methods did not manage to preserve the global colour characteristics of the site 3. The BDSD, LMVM, DWT, MTF-GLP, MTF-GLP-CBD, AWLP, SIHS-DWT and SIHS-DWFT methods were found to be more successful in this regard. It is also apparent in Figure 5 that the MTF-GLP and MTF-GLP-CBD methods produced blurry images in the site 3.

High visual quality of the colours does not always indicate that the used fusion method achieved to preserve the spectral quality. However, there may be colour artefacts that cannot be observed by the human eye. Since the qualitative evaluation is highly subjective and depends on both the monitor specifications and analyst's point of view, quantitative evaluation was conducted to ensure a more robust performance evaluation for the fusion methods used in this study.

5.2. Quantitative evaluation

Table 2 presents the spectral quality evaluation metric results for the test sites. In the table, the two fusion results with best metric values for each test site are highlighted with grey. As seen in the table, the proposed SIHS-DWT and SIHS-DWFT methods dominated the other fusion methods in keeping the colour content, especially in the sites 1 and 2. In the site 1, the best two RMSE, RASE, ERGAS, IW-SSIM, UIQI, MS-SSIM, SSIM, SID, SAM and *r* values of were achieved by the results of the proposed SIHS-DWT and SIHS-DWFT methods. The SIHS-DWT result got the RMSE, RASE, ERGAS, IW-SSIM, UIQI, MS-SSIM, SSIM, SID, SAM and *r* values of 23.977, 1.315, 2.444, 0.897, 0.532, 0.961, 0.961, 0.006, 1.311 and 0.986, correspondingly. On the other hand, the SIHS-DWFT result achieved the RMSE, RASE, ERGAS, IW-SSIM, UIQI,

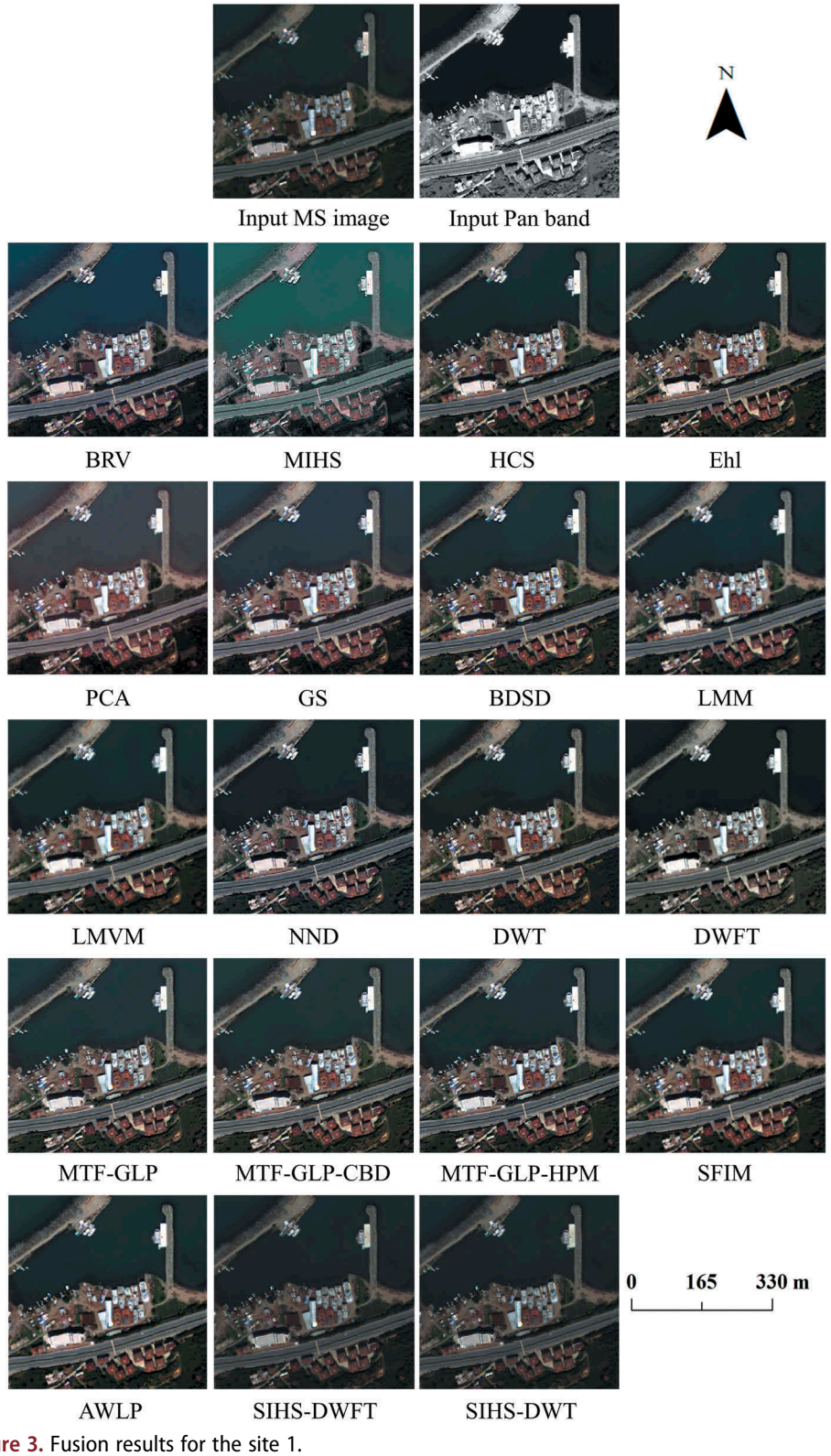

Figure 3. Fusion results for the site 1.

Figure 4. Fusion results for the site 2.

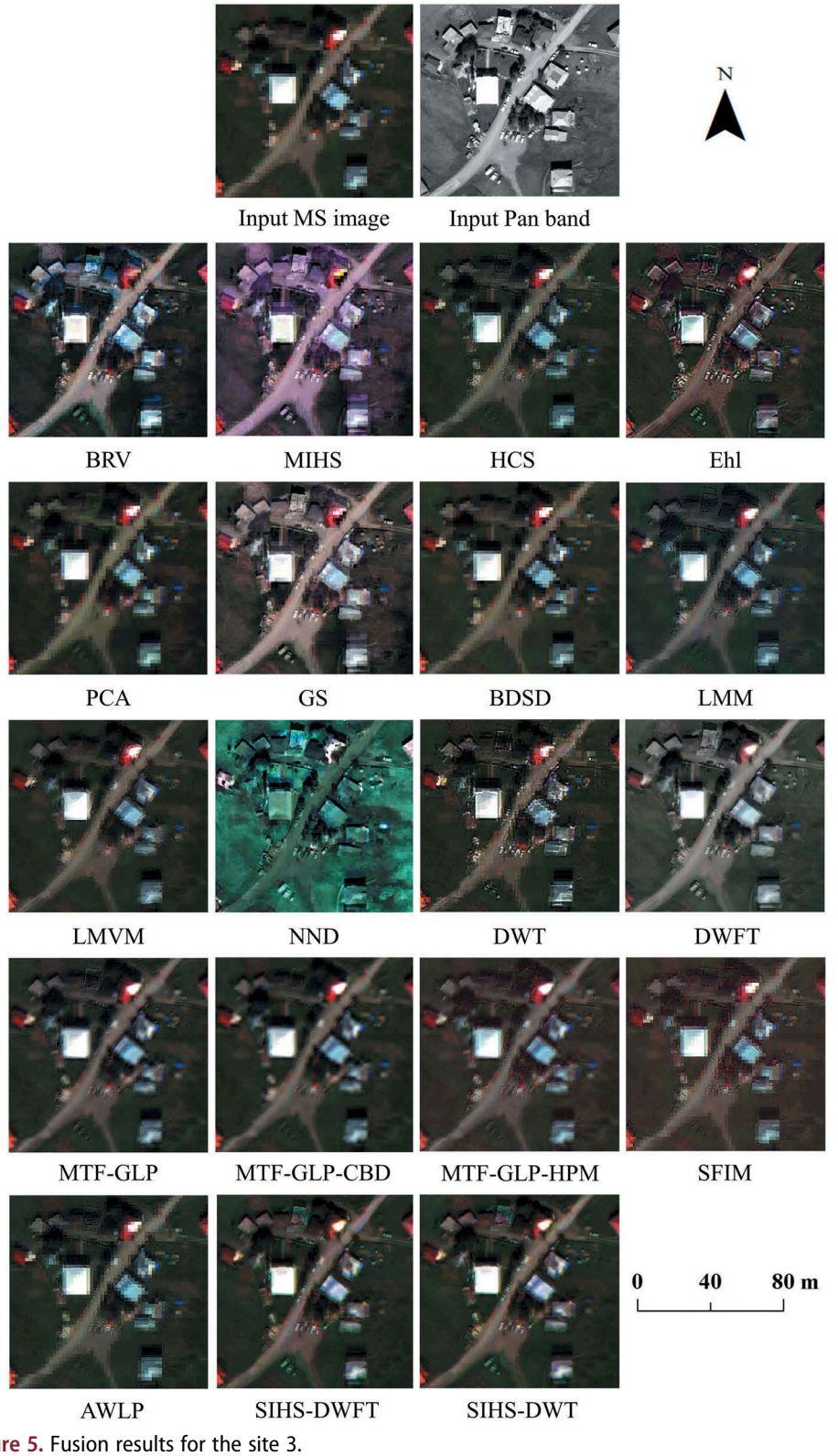

Figure 5. Fusion results for the site 3.

Table 2. Spectral quality evaluation metric values for all test sites.

Site	Method	RMSE	RASE	ERGAS	IW-SSIM	UIQI	MS-SSIM	SSIM	SID	SAM	*r*
1	**BRV**	100.377	5.526	10.377	0.292	0.079	0.553	0.498	0.031	5.734	0.734
	MIHS	100.301	5.500	10.464	0.287	0.073	0.551	0.488	0.053	6.926	0.737
	HCS	101.113	5.545	10.346	0.270	0.076	0.551	0.480	0.032	5.736	0.734
	Ehl	87.054	4.774	5.702	0.785	0.363	0.892	0.816	0.095	11.970	0.955
	PCA	75.296	4.129	9.260	0.788	0.384	0.878	0.841	0.215	5.223	0.926
	GS	101.335	5.557	10.442	0.301	0.079	0.562	0.499	0.067	7.487	0.746
	BDSD	103.264	5.663	10.621	0.298	0.075	0.555	0.501	0.061	6.927	0.747
	LMM	93.381	5.121	9.602	0.288	0.088	0.569	0.516	0.043	5.361	0.763
	LMVM	91.143	4.998	9.406	0.299	0.095	0.589	0.537	0.037	5.254	0.778
	NND	71.333	3.912	8.265	0.636	0.246	0.817	0.756	0.008	2.709	0.918
	DWT	47.525	2.606	4.991	0.698	0.198	0.839	0.809	0.045	3.876	0.943
	DWFT	50.667	2.778	5.101	0.836	0.468	0.913	0.894	0.017	5.551	0.950
	MTF-GLP	102.523	5.622	10.563	0.312	0.076	0.573	0.518	0.074	6.181	0.753
	MTF-GLP-CBD	100.090	5.489	10.090	0.314	0.080	0.577	0.524	0.067	6.028	0.758
	MTF-GLP-HPM	103.393	5.670	10.620	0.312	0.078	0.578	0.524	0.033	6.025	0.751
	SFIM	99.056	5.432	10.251	0.285	0.072	0.562	0.514	0.032	5.924	0.750
	AWLP	101.521	5.567	10.339	0.281	0.072	0.559	0.510	0.052	5.945	0.747
	SIHS-DWT	23.977	1.315	2.444	0.897	0.532	0.961	0.961	0.006	1.311	0.986
	SIHS-DWFT	22.034	1.208	2.157	0.954	0.727	0.981	0.978	0.003	2.171	0.990
2	**BRV**	85.177	7.243	5.570	0.586	0.348	0.808	0.422	0.007	2.740	0.806
	MIHS	83.693	7.117	5.566	0.575	0.345	0.801	0.415	0.010	3.281	0.798
	HCS	125.651	10.685	8.470	0.508	0.262	0.749	0.320	0.013	3.040	0.772
	Ehl	90.888	7.729	5.322	0.625	0.389	0.837	0.467	0.021	6.328	0.863
	PCA	73.483	6.249	4.777	0.638	0.387	0.848	0.469	0.009	3.150	0.859
	GS	84.405	7.177	5.583	0.593	0.353	0.819	0.429	0.011	3.483	0.819
	BDSD	100.997	8.588	6.629	0.557	0.326	0.801	0.389	0.013	4.587	0.837
	LMM	82.009	6.974	5.426	0.620	0.369	0.843	0.437	0.005	2.225	0.839
	LMVM	69.010	5.868	4.505	0.642	0.382	0.885	0.497	0.009	3.210	0.881
	NND	191.062	16.247	9.564	0.307	0.139	0.573	0.185	0.023	4.316	0.615
	DWT	93.231	7.928	6.107	0.567	0.312	0.803	0.382	0.018	4.764	0.795
	DWFT	65.323	5.555	4.242	0.721	0.536	0.898	0.603	0.020	4.947	0.890
	MTF-GLP	99.623	8.471	6.446	0.602	0.369	0.859	0.432	0.014	4.314	0.857
	MTF-GLP-CBD	100.423	8.539	6.447	0.605	0.371	0.860	0.435	0.015	4.473	0.858
	MTF-GLP-HPM	113.820	9.679	7.434	0.599	0.364	0.857	0.430	0.010	3.486	0.839
	SFIM	92.806	7.892	6.137	0.623	0.357	0.867	0.429	0.009	3.297	0.835
	AWLP	93.522	7.953	5.991	0.628	0.370	0.870	0.445	0.013	3.486	0.845
	SIHS-DWT	43.536	3.702	2.878	0.749	0.541	0.923	0.622	0.001	1.283	0.944
	SIHS-DWFT	59.343	5.046	4.160	0.749	0.563	0.903	0.631	0.011	1.806	0.914
3	**BRV**	151.223	6.799	11.993	0.112	0.023	0.205	0.203	0.091	10.543	0.417
	MIHS	149.775	6.733	13.289	0.098	0.021	0.179	0.155	0.225	12.085	0.436
	HCS	135.806	6.105	10.905	0.147	0.026	0.287	0.260	0.091	10.544	0.538
	Ehl	81.210	3.651	6.082	0.394	0.149	0.590	0.423	0.031	6.593	0.839
	PCA	210.155	9.448	8.887	0.446	0.148	0.571	0.513	0.185	10.607	0.612
	GS	149.991	6.743	12.527	0.106	0.022	0.192	0.178	0.235	11.697	0.433
	BDSD	146.855	6.602	11.813	0.154	0.035	0.299	0.297	0.125	12.154	0.534
	LMM	133.636	6.008	10.805	0.155	0.046	0.292	0.267	0.084	10.160	0.546
	LMVM	129.555	5.824	10.430	0.175	0.062	0.330	0.334	0.120	9.966	0.562
	NND	1347.942	60.596	32.939	0.065	0.032	0.131	0.069	0.260	4.585	0.231
	DWT	86.998	3.911	6.917	0.347	0.088	0.575	0.414	0.028	5.731	0.810
	DWFT	89.709	4.033	5.979	0.490	0.287	0.623	0.560	0.038	6.598	0.813
	MTF-GLP	132.896	5.975	10.672	0.182	0.078	0.318	0.309	0.131	10.410	0.559
	MTF-GLP-CBD	131.306	5.903	10.581	0.203	0.111	0.336	0.347	0.088	10.325	0.563
	MTF-GLP-HPM	706.690	317.706	680.043	0.169	0.076	0.302	0.301	0.354	11.125	0.424
	SFIM	467.464	21.016	72.797	0.141	0.025	0.278	0.256	0.354	11.516	0.438
	AWLP	136.921	6.156	10.913	0.152	0.027	0.296	0.277	0.110	10.654	0.539
	SIHS-DWT	76.974	3.461	4.670	0.574	0.334	0.719	0.648	0.018	5.351	0.890
	SIHS-DWFT	84.905	3.817	4.991	0.541	0.303	0.691	0.621	0.024	6.587	0.874

MS-SSIM, SSIM, SID, SAM and *r* values of 22.034, 1.208, 2.157, 0.954, 0.727, 0.981, 0.978, 0.003, 2.171 and 0.990, respectively. As can be seen, in the site 1, the colour qualities of the fused images obtained from the SIHS-DWT and SIHS-DWFT methods were significantly better than

the results of the other methods used. In the site 2, the proposed methods achieved the best two RMSE, RASE, ERGAS, IW-SSIM, UIQI, MS-SSIM, SSIM, SAM and *r* values. As seen in Table 2, the SIHS-DWT result got the RMSE, RASE, ERGAS, IW-SSIM, UIQI, MS-SSIM, SSIM, SID, SAM and *r* values of 43.536, 3.702, 2.878, 0.749, 0.541, 0.923, 0.622, 0.001, 1.283 and 0.944, respectively. On the other hand, in the site 2, the RMSE, RASE, ERGAS, IW-SSIM, UIQI, MS-SSIM, SSIM, SAM and *r* values of 59.343, 5.046, 4.160, 0.749, 0.563, 0.903, 0.631, 1.806 and 0.914, correspondingly. It is obvious that the metric values achieved by the SIHS-DWT and SIHS-DWFT results were significantly better than those obtained from the results of the other fusion methods used. In the site 3, the best two ERGAS, IW-SSIM, UIQI, MS-SSIM, SSIM, SID and *r* values were obtained by the proposed methods. The SIHS-DWT result achieved the RMSE, RASE, ERGAS, IW-SSIM, UIQI, MS-SSIM, SSIM, SID, SAM and *r* values of 76.974, 3.461, 4.670, 0.574, 0.334, 0.719, 0.648, 0.018, 5.351 and 0.890, respectively. In the site 3, the ERGAS, IW-SSIM, UIQI, MS-SSIM, SSIM, SID and *r* values of 4.991, 0.541, 0.303, 0.691, 0.621, 0.024 and 0.874 were obtained by the SIHS-DWFT result, correspondingly. It can be concluded that the SIHS-DWT and SIHS-DWFT methods led to superior metric values in the site 3. It is obvious that the SIHS-DWT and SIHS-DWFT methods managed to find the optimum band weights that achieved the optimum spectral fidelity. Matching the histogram of the input Pan band to that of the intensity component was the other factor that helped preserve the colour content. The biggest advantage of the SIHS-DWT and SIHS-DWFT methods is that they are easy to implement and use only one user-defined parameter (i.e. ecosystem size), which enables the analysts to obtain the optimum results in a short span of time without being have to try different values for different parameters. Another advantage of the SIHS-DWT and SIHS-DWFT methods is that they converge very fast. The reason for this convergence speed is that the commensalism operator uses the optimum solution of a generation as a reference to specify promising regions around the optimum solution. The parasitism operator ensures the naturalness of the ecosystem and enables the SIHS-DWT and SIHS-DWFT methods to achieve the optimum solutions from all parts of the ecosystem. Increasing the ecosystem size parameter helps obtain more reasonable band weights, increasing the spectral quality. The wavelet transform is very successful in separating the colour and spatial details; however, it may cause spatial detail loss due to the fact that it extracts the spatial details only in horizontal, vertical and diagonal directions. The SIHS-DWT and SIHS-DWFT methods ensure the spectral and spatial consistency by substituting the approximation component obtained from the intensity component by its average with the approximation component obtained from the histogram-matched Pan band. It is also possible to achieve a better colour quality by using a greater weight for the approximation component obtained from the intensity component, and a better spatial quality by using a greater weight for the approximation component obtained from the histogram-matched Pan band. This study used equal weights for both components to achieve a compromise between the spectral and spatial quality.

As seen in Table 2, the DWFT results got the best global spectral metric values after the SIHS-DWT and SIHS-DWFT methods. The DWFT method performed best in the site 1 with the RMSE, RASE, ERGAS, IW-SSIM, UIQI, MS-SSIM, SSIM, SID, SAM and *r* values of 50.667, 2.778, 5.101, 0.836, 0.468, 0.913, 0.894, 0.017, 5.551 and 0.950, respectively. The DWFT method is based on the DWT and does not employ a downsampling process, which leads to the same image size after transformation. The DWFT method, on the other hand, does not consider regional characteristics, since each part of the scene has its own local

features. This is a huge disadvantage for this method. Unlike the DWFT, the DWT method applies downsampling, which changes the size of the images. This change is likely to have a negative effect on the fusion result, especially when the input images are not perfectly registered.

The Ehl method, which provided spectrally consistent images in all test sites (see Table 2), filters the intensity and Pan spectrums in fourier domain, which helps retain the colour characteristics of the input MS image and transfer the spatial details of the input Pan band. The Ehl method applies an IHS transform, which attaches importance on the IHS transform procedure used. It also uses successive three-band selections to perform the IHS transform until all bands are fused (Klonus and Ehlers 2009), which increases the computation time. A more efficient IHS transform procedure can be used to alleviate the workload. One of the biggest advantages of the Ehl method is that it allows the users to change the filter design to achieve maximum colour preservation or spatial enhancement. If maximum colour quality is needed, then the filter is shifted to the higher frequencies of the power spectrum to suppress the spatial information. However, if the focus is on maximum spatial detail quality, then the filter is shifted to the lower frequencies to include more spatial detail content. A compromise between the colour preservation and spatial enhancement can be found by moving the cut-off frequency, as done in this study.

Table 2 shows that the LMM and LMVM methods provided satisfactory colour preservation in all test sites. In addition, they showed similar performances. These methods aim to match the local intensities through matching windows, which places emphasis on the selection of the optimum window size. Smaller window sizes result in less colour distortion, whereas larger window sizes produce sharper images. In order to make a compromise between the colour and spatial quality, this study used a window whose size was the minimum odd number that is greater than the ratio between the input MS and Pan bands. This approach allowed for controlling the frequency distribution at a local scale.

As seen in Table 2, the PCA is one of the other methods that provided satisfactory colour preservation. This method is a statistical procedure, which means that its performance is dependent on both the scene characteristics and statistical relevance between the input images. Unlike the input images of the sites 2 and 3, the input images of the site 1 were acquired from the same sensor, which is why the PCA method yielded generally better global spectral metric values in the site 1, compared to the sites 2 and 3. The PCA result, in the site 1, got the RMSE, RASE, ERGAS, IW-SSIM, UIQI, MS-SSIM, SSIM, SID, SAM and r values of 75.296, 4.129, 9.260, 0.788, 0.384, 0.878, 0.841, 0.215, 5.223 and 0.926, respectively. The GS, another statistical procedure similar to the PCA, did not manage to keep the colour content of the input MS images (see Table 2 and Figures 3–5). The GS method simulates a low-resolution Pan band, which is used as the first component of the intermediary image to which the GS is applied. However, how to estimate the optimum weights for the input MS and Pan bands to compute the simulated Pan band is still not clear. It is possible to estimate the band weights either from the sensor's spectral sensitivity curves or from linear regression methods (Pohl and van Genderen 2016). A low-resolution Pan band can also be calculated by averaging the input MS bands. It is also possible to define another low-resolution Pan band, instead of computing a new one. Since there were no other low-resolution Pan band for the test sites, this study generated low-resolution Pan bands by averaging the input MS bands. The GS method changed the

spectral interrelation between different objects as can be observed in Figures 3–5. Both the PCA and GS methods performed worst in the site 3, compared to the other sites. This was because the spectral overlap between the input MS and Pan bands was the smallest in the site 3.

Table 2 shows that, in all test sites, the MTF-GLP, MTF-GLP-CBD and AWLP methods showed an overall performance in keeping the colour content, whereas the MTF-GLP-HPM method caused a greater amount of spectral distortion that cannot be observed by the human eye (see Figures 3–5). The MTF-GLP method designs the GLP reduction filter by using the MTFs of the imaging sensor. The Pan band is reduced with the MTF filter and the histogram-matched Pan band is interpolated. The low-resolution Pan band is subtracted from the original Pan band to obtain the spatial detail information to be added into the input MS bands. Producing the detail information this way caused some colour distortion and blurry effects, especially where the frequency changed drastically (See Figure 4). The MTF-GLP-HPM method follows the same steps as the MTF-GLP method, except for the high-pass modulation injection procedure, which is based on simply multiplying the spatial details. This procedure deteriorated the colour content, as can be seen from the metric values given in Table 2. A procedure that considers the regional characteristics may be of help to better keep the colour features. The MTF-GLP-CBD method optimizes the spatial detail injection coefficients by least square fitting. The image is patched in nonoverlapping zones to locally optimize the injection coefficients. This approach enabled the preservation of the colour characteristics to some extent. The AWLP method utilizes the IHS transform to obtain an intensity component to be used to modify the histogram of the Pan band, which led to fair spectral metric values in all test sites (see Table 2). The AWLP method also relatively injects the spatial details into the MS bands, which helped keep the chromatic relationship between the MS bands to a certain extent.

As seen in Table 2, the BRV, SFIM and NND methods were found to deteriorate the colour characteristics in all test sites. The BRV method normalizes the MS image by dividing it with an intensity component produced by summing all MS bands. However, this is not always efficient for all types of input images since each spectral band should have its own weight. Estimating the band weights in a more efficient way would enable the BRV method to better preserve the colour characteristics. The SFIM method employs a low-pass filter on the input Pan band. The input Pan band is then divided by the smoothed Pan band to extract the spatial details. Hence, plenty of attention should be paid to design the low-pass filter used. Otherwise, spectral distortion or spatial detail loss would be inevitable, especially for terrains with high colour frequency. The challenge in finding the optimum low-pass filter design was the reason for the spectral distortion in the site 3 (see Table 2 and Figure 5). Greater filter sizes lead to smoother images, causing colour distortion in the final fused image. Hence, a compromise should be found between the colour quality and spatial fidelity. More efficient smoothing filters such as Gaussian or Kuwahara may be of help to keep the colour content while preserving the spatial details. The NND method considers only positive diffusion weights caused by the exponent, which was the main reason for the low spectral fidelity of the NND results of all test sites. The NND method also uses two parameters, which are the spatial smoothness factor and intensity smoothness factor. Greater intensity smoothness factor values lead to higher spectral fidelity, but poorer spatial detail quality. The analysts have to try different

values for these parameters to obtain the optimum spectral and spatial quality, which is the biggest disadvantage of the NND method. A compromise can be said to found between the spatial smoothness factor and intensity smoothness factor parameters in the sites 1 and 2; however, it was very challenging to find the optimum values for these parameters in the site 3. This was the main reason for the drastic colour change in this site (see Figure 5).

Table 2 shows that the BDSD, HCS and MIHS methods got the worst metric values in all test sites. The HCS method uses the ratio between the Pan band and a smoothed version of the Pan band in order to extract the spatial detail information used to adjust the intensity component. This, of course, attributes importance to the smoothing procedure used, just as in the SFIM and MTF-based methods. The HCS method, on the other hand, performs histogram matching between the intensity and adjusted intensity components, which absorbs the spatial details to a certain extent, as in the site 1 and 3 (see Figures 3 and 5). The MIHS method preserves the colour features best if the input MS and Pan bands cover the same part of the electromagnetic spectrum, which was the main reason that the MIHS method performed worse in the site 3, compared to the other sites.

Image fusion aims at transferring the spatial details of the input Pan band while keeping the colour characteristics of the input MS image. Hence, in addition to colour fidelity, spatial fidelity should also be evaluated. Table 3 shows the spatial quality metric values computed between the input Pan band and fused bands. Note that the best two metric values are highlighted with grey colour in the table. As seen in Table 3, the proposed SIHS-DWT and SIHS-DWFT methods achieved very good spatial metric values in all test sites. In fact, these methods did not manage to transfer the spatial details as successful as they kept the colour content. As seen in Table 2, the SIHS-DWT and SIHS-DWFT methods dominated the others in terms of colour quality, which was not true for spatial quality (see Table 3). The reason for this was that the proposed methods were designed to achieve the optimum spectral quality by using the ERGAS metric as the fitness criterion. Table 3 shows that the DWFT, SIHS-DWT, Ehl and SIHS-DWFT methods got the best spatial quality metric values in all test sites. On the other hand, the BDSD, AWLP, SFIM and HCS methods got the worst spatial quality metric values from the fused images produced with the datasets used.

Too many performance metrics were used in this study to assess the quality of a large number of image fusion methods, which made it very challenging to interpret the performance of the image fusion methods used. Hence, a performance score was given to each fusion result with respect to its metric value. Since a total of 19 image fusion methods were used in this study, each fusion result was given a score between 1 and 19. For each metric, the best fusion result got the score of 19, whereas the worst one got the score of 1. It should also be noted that the performance scores were given considering only the quantitative evaluation results. This was because the qualitative evaluation is highly subjective and depends highly on the analyst's point of view, which negatively affects the robustness of a fair comparison. Gungor (2008), Yilmaz and Gungor (2016a, 2016b), Kwan et al. (2017) and Yilmaz, Serifoglu Yilmaz, and Gungor (2019) also gave performance scores to each fusion result to ensure a fair comparison. Tables 4 and 5 show

Table 3. Spatial quality evaluation metric values for all test sites.

Site	Method	IW-SSIM	r	SSIM	r_s
1	**BRV**	0.241	0.587	0.361	0.139
	MIHS	0.239	0.580	0.375	0.137
	HCS	0.196	0.596	0.341	0.117
	Ehl	0.775	0.856	0.737	0.888
	PCA	0.744	0.827	0.697	0.629
	GS	0.240	0.609	0.381	0.153
	BDSD	0.227	0.607	0.343	0.142
	LMM	0.199	0.620	0.347	0.178
	LMVM	0.210	0.638	0.761	0.241
	NND	0.706	0.854	0.667	0.342
	DWT	0.664	0.830	0.630	0.533
	DWFT	0.832	0.954	0.787	0.928
	MTF-GLP	0.258	0.625	0.736	0.124
	MTF-GLP-CBD	0.253	0.627	0.741	0.129
	MTF-GLP-HPM	0.256	0.620	0.735	0.121
	SFIM	0.193	0.609	0.745	0.121
	AWLP	0.191	0.606	0.742	0.128
	SIHS-DWT	0.724	0.862	0.864	0.822
	SIHS-DWFT	0.696	0.874	0.857	0.829
2	**BRV**	0.707	0.768	0.615	0.516
	MIHS	0.725	0.783	0.632	0.522
	HCS	0.699	0.774	0.565	0.447
	Ehl	0.812	0.872	0.838	0.951
	PCA	0.776	0.854	0.801	0.942
	GS	0.719	0.789	0.628	0.529
	BDSD	0.695	0.770	0.608	0.511
	LMM	0.693	0.751	0.597	0.516
	LMVM	0.693	0.767	0.836	0.522
	NND	0.307	0.409	0.205	0.145
	DWT	0.696	0.802	0.687	0.839
	DWFT	0.853	0.935	0.840	0.974
	MTF-GLP	0.710	0.797	0.766	0.455
	MTF-GLP-CBD	0.706	0.796	0.764	0.455
	MTF-GLP-HPM	0.701	0.785	0.770	0.438
	SFIM	0.636	0.730	0.753	0.440
	AWLP	0.639	0.739	0.752	0.437
	SIHS-DWT	0.769	0.850	0.770	0.959
	SIHS-DWFT	0.775	0.852	0.751	0.926
3	**BRV**	0.076	0.281	0.125	0.230
	MIHS	0.066	0.259	0.095	0.222
	HCS	0.056	0.188	0.128	0.203
	Ehl	0.438	0.494	0.312	0.896
	PCA	0.293	0.751	0.241	0.491
	GS	0.074	0.278	0.108	0.235
	BDSD	0.055	0.190	0.138	0.198
	LMM	0.059	0.193	0.132	0.230
	LMVM	0.064	0.202	0.603	0.309
	NND	0.083	0.074	0.037	0.053
	DWT	0.345	0.459	0.293	0.472
	DWFT	0.687	0.818	0.457	0.939
	MTF-GLP	0.075	0.204	0.604	0.295
	MTF-GLP-CBD	0.070	0.199	0.614	0.392
	MTF-GLP-HPM	0.068	0.117	0.597	0.233
	SFIM	0.049	0.124	0.583	0.167
	AWLP	0.054	0.192	0.588	0.196
	SIHS-DWT	0.545	0.637	0.634	0.835
	SIHS-DWFT	0.548	0.654	0.632	0.772

the spectral and spatial performance scores given to each fusion method used, respectively. Note that the best two scores for each metric are highlighted with grey colour in the Tables.

6. Conclusion

This study proposed two hybrid image fusion methodologies based on the IHS and DWT/DWFT methods. The proposed methods utilize the SOS optimization algorithm to find the optimum band weights used to generate the optimum intensity component, which plays a significant role in the success of the fusion process. The spectral and spatial quality of the fused images obtained by the proposed SIHS-DWT and SIHS-DWFT methods were compared against those of several image fusion methods, including the BRV, MIHS, HCS, Ehl, PCA, GS, BDSD, LMM, LMVM, NND, DWT, DWFT, MTF-GLP, MTF-GLP-CBD, MTF-GLP-HPM, SFIM and AWLP. The spectral qualities of the fused images were compared qualitatively and quantitatively. The RMSE, RASE, ERGAS, IW-SSIM, UIQI, MS-SSIM, SSIM, SID, SAM and r metrics were used for spectral quality evaluation, whereas the IW-SSIM, r, SSIM and r_s metrics were used for spatial quality evaluation.

Figure 6 presents the average spectral and spatial performance scores computed from the scores given in Tables 4 and 5. As seen in the figure, the proposed SIHS-DWT and SIHS-DWFT methods led to the optimum colour quality with average spectral performance scores of 18.6 and 18.0, respectively. The DWFT, LMVM, Ehl and PCA methods were found to be the other methods that achieved to preserve the colour characteristics with average performance scores of 15.4, 13.0, 12.9 and 12.9, respectively. Figure 6 also shows that the DWT, LMM and MTF-GLO-CBD methods presented a fair spectral fidelity in all test sites. It was also concluded that the HCS, MIHS and BDSD methods caused the greatest amount of colour distortion with average spectral performance scores of 5.6, 5.5 and 5.2, respectively. When it comes to spatial quality, the proposed SIHS-DWT and SIHS-DWFT methods were among the most successful ones. As seen in Figure 6, the DWFT, SIHS-DWT, Ehl, SIHS-DWFT and PCA methods were the most successful ones in transferring the spatial details with average spatial performance scores of 18.2, 16.6, 16.2, 16.0 and 14.6, respectively. Figure 6 also depicts that the DWT, MTF-GLP, MTF-GLP-CBD and LMVM

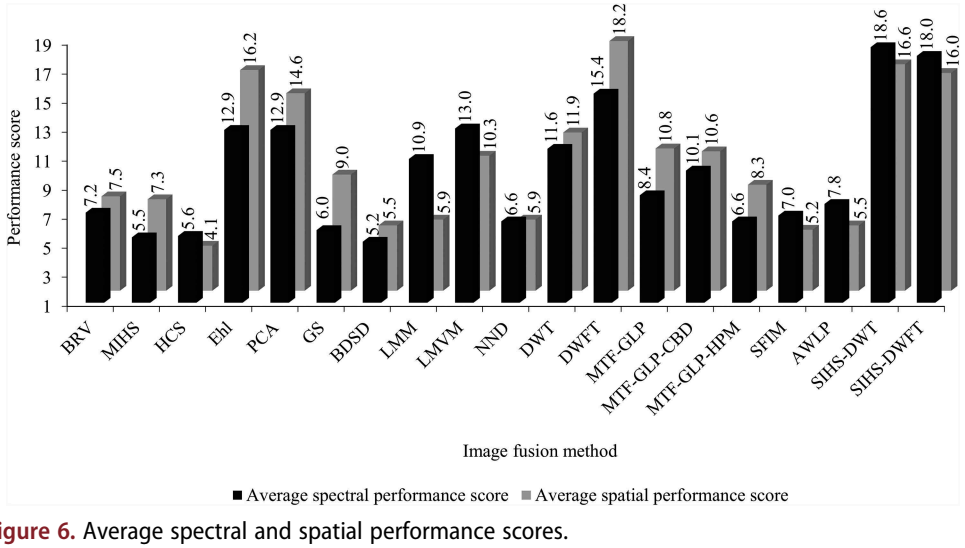

Figure 6. Average spectral and spatial performance scores.

Table 4. Spectral performance scores given to each fusion method.

Site	Method	RMSE	RASE	ERGAS	IW-SSIM	UIQI	MS-SSIM	SSIM	SID	SAM	*r*
1	**BRV**	7	7	6	6	8	3	3	15	11	1
	MIHS	8	8	4	4	3	1	2	7	4	3
	HCS	6	6	7	1	5	1	1	13	10	1
	Ehl	13	13	15	15	15	16	15	2	1	17
	PCA	14	14	13	16	16	15	16	1	15	14
	GS	5	5	5	9	8	6	4	4	2	4
	BDSD	2	2	1	7	4	4	5	6	3	5
	LMM	11	11	11	5	11	8	8	10	13	11
	LMVM	12	12	12	8	12	12	12	11	14	12
	NND	15	15	14	13	14	13	13	17	17	13
	DWT	17	17	17	14	13	14	14	9	16	15
	DWFT	16	16	16	17	17	17	17	16	12	16
	MTF-GLP	3	3	3	10	5	9	9	3	5	9
	MTF-GLP-CBD	9	9	10	12	10	10	10	4	6	10
	MTF-GLP-HPM	1	1	2	10	7	11	10	12	7	8
	SFIM	10	10	9	3	1	6	7	13	9	7
	AWLP	4	4	8	2	1	5	6	8	8	5
	SIHS-DWT	18	18	18	18	18	18	18	18	19	18
	SIHS-DWFT	19	19	19	19	19	19	19	19	18	19
2	**BRV**	11	11	11	6	6	6	6	17	16	5
	MIHS	13	13	12	5	5	3	5	12	12	4
	HCS	2	2	2	2	2	2	2	7	15	2
	Ehl	10	10	14	13	16	8	14	2	1	15
	PCA	15	15	15	15	15	10	15	14	14	14
	GS	12	12	10	7	7	7	7	10	10	6
	BDSD	4	4	4	3	4	3	4	7	4	8
	LMM	14	14	13	11	10	9	12	18	17	9
	LMVM	16	16	16	16	14	16	16	14	13	16
	NND	1	1	1	1	1	1	1	1	6	1
	DWT	8	8	8	4	3	5	3	4	3	3
	DWFT	17	17	17	17	17	17	17	3	2	17
	MTF-GLP	6	6	6	9	10	12	10	6	7	12
	MTF-GLP-CBD	5	5	5	10	13	13	11	5	5	13
	MTF-GLP-HPM	3	3	3	8	9	11	9	12	8	9
	SFIM	9	9	7	12	8	14	7	14	11	7
	AWLP	7	7	9	14	12	15	13	7	8	11
	SIHS-DWT	19	19	19	18	18	19	18	19	19	19
	SIHS-DWFT	18	18	18	18	19	18	19	10	18	18
3	**BRV**	5	5	6	4	3	4	4	11	9	2
	MIHS	7	7	4	2	1	2	2	5	2	5
	HCS	10	10	9	6	5	6	6	11	8	8
	Ehl	18	18	16	15	16	16	15	16	15	17
	PCA	4	4	14	16	15	14	16	6	7	14
	GS	6	6	5	3	2	3	3	4	3	4
	BDSD	8	8	7	8	8	9	9	8	1	7
	LMM	11	11	10	9	9	7	7	14	12	10
	LMVM	14	14	13	11	10	12	12	9	13	12
	NND	1	2	3	1	7	1	1	3	19	1
	DWT	16	16	15	14	13	15	14	17	17	15
	DWFT	15	15	17	17	17	17	17	15	14	16
	MTF-GLP	12	12	11	12	12	11	11	7	10	11
	MTF-GLP-CBD	13	13	12	13	14	13	13	13	11	13
	MTF-GLP-HPM	2	1	1	10	11	10	10	1	5	3
	SFIM	3	3	2	5	4	5	5	1	4	6
	AWLP	9	9	8	7	6	8	8	10	6	9
	SIHS-DWT	19	19	19	19	19	19	19	19	18	19
	SIHS-DWFT	17	17	18	18	18	18	18	18	16	18

methods presented a satisfying spatial fidelity in all test sites. The BDSD, AWLP, SFIM and HCS methods were found to cause the lowest spatial quality with average spatial performance scores of 5.5, 5.5, 5.2 and 4.1, respectively.

Table 5. Spatial performance scores given to each fusion method.

Site	Method	IW-SSIM	r	SSIM	r_s
1	**BRV**	9	2	4	8
	MIHS	7	1	5	7
	HCS	3	3	1	1
	Ehl	18	16	12	18
	PCA	17	13	9	15
	GS	8	6	6	10
	BDSD	6	5	2	9
	LMM	4	8	3	11
	LMVM	5	12	16	12
	NND	15	15	8	13
	DWT	13	14	7	14
	DWFT	19	19	17	19
	MTF-GLP	12	10	11	4
	MTF-GLP-CBD	10	11	13	6
	MTF-GLP-HPM	11	8	10	2
	SFIM	2	6	15	2
	AWLP	1	4	14	5
	SIHS-DWT	16	17	19	16
	SIHS-DWFT	14	18	18	17
2	**BRV**	11	6	5	9
	MIHS	14	9	7	11
	HCS	8	8	2	5
	Ehl	18	18	18	17
	PCA	17	17	16	16
	GS	13	11	6	13
	BDSD	6	7	4	8
	LMM	4	4	3	9
	LMVM	4	5	17	11
	NND	1	1	1	1
	DWT	7	14	8	14
	DWFT	19	19	19	19
	MTF-GLP	12	13	13	6
	MTF-GLP-CBD	10	12	12	6
	MTF-GLP-HPM	9	10	14	3
	SFIM	2	2	11	4
	AWLP	3	3	10	2
	SIHS-DWT	15	15	14	18
	SIHS-DWFT	16	16	9	15
3	**BRV**	12	13	4	7
	MIHS	7	11	2	6
	HCS	4	4	5	5
	Ehl	16	15	10	18
	PCA	14	18	8	15
	GS	10	12	3	10
	BDSD	3	5	7	4
	LMM	5	7	6	7
	LMVM	6	9	15	12
	NND	13	1	1	1
	DWT	15	14	9	14
	DWFT	19	19	11	19
	MTF-GLP	11	10	16	11
	MTF-GLP-CBD	9	8	17	13
	MTF-GLP-HPM	8	2	14	9
	SFIM	1	3	12	2
	AWLP	2	6	13	3
	SIHS-DWT	17	16	19	17
	SIHS-DWFT	18	17	18	16

As can be clearly seen, the proposed SIHS-DWT and SIHS-DWFT methods combined the superiorities of the IHS, DWT/DWFT and SOS algorithms. It was also concluded that the SIHS-DWT and SIHS-DWFT methods kept the colour characteristics regardless of the

Table 6. Advantages and disadvantages/limitations of the SIHS-DWT and SIHS-DWFT methods.

Advantages	Disadvantages/Limitations
• Able to handle large spatial resolution difference between the input images	• Hard to choose the best ecosystem size parameter
• Able to search in a very large parameter space	• Hard to choose the optimum weights for the intensity and Pan approximations
• Able to optimize the intensity component	
• Fast convergence	
• Easy to implement	
• Using only one user-defined parameter	
• No algorithm-specific constraints	

spatial resolution between the input MS bands. Another important conclusion drawn from the quantitative evaluation results is that the SIHS-DWT and SIHS-DWFT methods showed a very good performance with both singlesensor and multisensor input images. The advantages and disadvantages/limitations of the SIHS-DWT and SIHS-DWFT methods are summarized in Table 6.

Generally speaking, the MRA-based methods were found to achieve the optimum colour quality and spatial detail content. On the other hand, the CS-based methods caused the greatest amount of colour distortion, whereas the CB methods produced the images with lowest spatial fidelity.

This study showed the effectiveness of the SOS metaheuristic algorithm in increasing the performance of the hybrid image fusion methods. Further studies will focus on using the metaheuristic algorithms to increase the performances of some other image fusion methods.

Acknowledgements

This study was partly supported by the Scientific and Technological Research Council of Turkey (TUBITAK) (no: 111Y296). We would like to express our sincere gratitude to the anonymous reviewers for their constructive comments and suggestions.

Disclosure statement

No potential conflict of interest was reported by the authors.

Funding

This work was supported by the Scientific and Technological Research Council of Turkey (TUBITAK) [111Y296].

ORCID

Cigdem Serifoglu Yilmaz http://orcid.org/0000-0002-9738-5124
Volkan Yilmaz http://orcid.org/0000-0003-0685-8369
Oguz Güngör http://orcid.org/0000-0002-3280-5466

References

Aiazzi, B., L. Alparone, S. Baronti, A. Garzelli, and M. Selva. 2006. "MTF-tailored Multiscale Fusion of High-resolution MS and Pan Imagery." *Photogrammetric Engineering & Remote Sensing* 72 (5): 591–596. doi:10.14358/PERS.72.5.591.

Alparone, L., B. Aiazzi, S. Baronti, A. Garzelli, and F. Nencini. 2006. "Information-Theoretic Image Fusion Assessment without Reference." ESA-EUSC 2006: Image Information Mining for Security and Intelligence, Torrejon Air Base, Madrid, Spain.

Alparone, L., L. Wald, J. Chanussot, C. Thomas, P. Gamba, and L. M. Bruce. 2007. "Comparison of Pansharpening Algorithms: Outcome of the 2006 GRS-S Data-Fusion Contest." *IEEE Transactions on Geoscience and Remote Sensing* 45 (10): 3012–3021. doi:10.1109/TGRS.2007.904923.

Chavez, P. S., and A. Y. Kwarteng. 1989. "Extracting Spectral Contrast in Landsat Thematic Mapper Image Data Using Selective Principal Component Analysis." *Photogrammetric Engineering & Remote Sensing* 55: 339–348.

Cheng, M. Y., and D. Prayogo. 2014. "Symbiotic Organisms Search: A New Metaheuristic Optimization Algorithm." *Computers & Structures* 139: 98–112. doi:10.1016/j.compstruc.2014.03.007.

de Béthune, S., F. Muller, and M. Binard. 1997. "Adaptive Intensity Matching Filters: A New Tool for Multiresolution Data Fusion." Proceedings of the Multi-Sensor Systems and Data Fusion for Telecommunications, Remote Sensing and Radar, Lisbon, Portugal.

Ehlers, M. 2004. "Spectral Characteristics Preserving Image Fusion Based on Fourier Domain Filtering." *Remote Sensing for Environmental Monitoring, GIS Applications, and Geology IV, Proceedings of SPIE* 5574 (1): 1–13. doi:10.1117/12.565160.

Elkaffas, S. M., T. A. El-Tobely, A. M. Ragheb, and F. A. El-Samie. 2006. "An Integrated IHS and DWFT Fusion Technique for Improving the Spectral Quality of Remote Sensing Images." 2nd International Computer Engineering Conference (ICENCO), Cairo, Egypt, pp. 54–61. doi: 10.1016/j.jhsb.2006.09.001

El-Samie, F. E. A., M. M. Hadhoud, and S. E. El-Khamy. 2012. *Image Super-resolution and Applications*. Boca Raton, FL: CRC press.

Garzelli, A., and F. Nencini. 2006a. "Fusion of Panchromatic and Multispectral Images by Genetic Algorithms." IEEE International Conference on Geoscience and Remote Sensing Symposium (IGARSS), Denver, CO, USA, pp. 3810–3813.

Garzelli, A., and F. Nencini. 2006b. "PAN-sharpening of Very High Resolution Multispectral Images Using Genetic Algorithms." *International Journal of Remote Sensing* 27 (15): 3273–3292. doi:10.1080/01431160600554991.

Garzelli, A., F. Nencini, and L. Capobianco. 2008. "Optimal MMSE Pan Sharpening of Very High Resolution Multispectral Images." *IEEE Transactions on Geoscience and Remote Sensing* 46 (1): 228–236. doi:10.1109/TGRS.2007.907604.

Ghassemian, H. 2016. "A Review of Remote Sensing Image Fusion Methods." *Information Fusion* 32: 75–89. doi:10.1016/j.inffus.2016.03.003.

Gonzalez, R. C., and R. E. Woods. 2007. *Digital Image Processing*. 3rd ed. London, UK: Pearson.

Gungor, O. 2008. "Multi sensor multi resolution image fusion." PhD thesis, Purdue University.

Hallada, W. A., and S. Cox. 1983. "Image Sharpening for Mixed Spatial and Spectral Resolution Satellite Systems." 17th International Symposium on Remote Sensing of Environment, Ann Arbor, MI, pp. 1023–1032.

Haydn, R., G. W. Dalke, J. Henkel, and J. E. Bare. 1982. "Application of the IHS Color Transform to the Processing of Multi-sensor Data and Image Enhancement." International Symposium on Remote Sensing of Environment, First Thematic Conference: 'Remote Sensing of Arid and Semi-arid Lands', Cairo, Egypt, pp. 599–616.

Holland, H. 1975. *Adaptation in Natural and Artificial Systems*. Ann Arbor: University of Michigan Press.

Imani, M. 2018. "Band Dependent Spatial Details Injection Based on Collaborative Representation for Pansharpening." *IEEE Journal of Selected Topics in Applied Earth Observations and Remote Sensing* 11 (12): 4994–5004. doi:10.1109/JSTARS.2018.2851791.

Klonus, S., and M. Ehlers. 2007. "Image Fusion Using the Ehlers Spectral Characteristics Preserving Algorithm." *GIScience & Remote Sensing* 44: 93–116. doi:10.2747/1548-1603.44.2.93.

Klonus, S., and M. Ehlers. 2009. "Performance of Evaluation Methods in Image Fusion." 12th IEEE International Conference on Information Fusion, Seattle, WA, USA, pp. 1409–1416.

Kwan, C., B. Budavari, A. C. Bovik, and G. Marchisio. 2017. "Blind Quality Assessment of Fused WorldView-3 Images by Using the Combinations of Pansharpening and Hypersharpening Paradigms." *IEEE Geoscience and Remote Sensing Letters* 14 (10): 1835–1839. doi:10.1109/LGRS.2017.2737820.

Laben, C. A., and B. V. Brower. 2000. "Process for Enhancing the Spatial Resolution of Multispectral Imagery Using Pan-sharpening." U.S. Patent No: 6,011,875.

Li, H., B. S. Manjunath, and S. K. Mitra. 1995. "Multisensor Image Fusion Using the Wavelet Transform." *Graphical Models and Image Processing* 57 (3): 235–245. doi:10.1006/gmip.1995.1022.

Li, S., J. T. Kwok, and Y. Wang. 2002. "Using the Discrete Wavelet Frame Transform to Merge Landsat TM and SPOT Panchromatic Images." *Information Fusion* 3 (1): 17–23. doi:10.1016/S1566-2535(01)00037-9.

Liu, J. G. 2000. "Smoothing Filter-based Intensity Modulation: A Spectral Preserve Image Fusion Technique for Improving Spatial Details." *International Journal of Remote Sensing* 21 (18): 3461–3472. doi:10.1080/014311600750037499.

Masoudi, R., and P. Kabiri. 2014. "New Intensity-hue-saturation Pan-sharpening Method Based on Texture Analysis and Genetic Algorithm-adaption." *Journal of Applied Remote Sensing* 8: 1. doi:10.1117/1.JRS.8.083640.

Munechika, C. K., J. S. Warnick, C. Salvaggio, and J. R. Schott. 1993. "Resolution Enhancement of Multispectral Image Data to Improve Classification Accuracy." *Photogrammetric Engineering & Remote Sensing* 59 (1): 67–72.

Niazi, S. M. N., M. M. Zade, and F. S. Zadeh. 2016. "A Novel IHS-GA Fusion Method Based on Enhancement Vegetated Area." *Journal of Geomatics Science and Technology* 6 (1): 235–248.

Nunez, J., X. Otazu, O. Fors, A. Prades, V. Pala, and R. Arbiol. 1999. "Multiresolution-based Image Fusion with Additive Wavelet Decomposition." *IEEE Transactions on Geoscience and Remote Sensing* 37 (3): 1204–1211. doi:10.1109/36.763274.

Otazu, X., M. González-Audícana, O. Fors, and J. Núñez. 2005. "Introduction of Sensor Spectral Response into Image Fusion Methods. Application to Wavelet-based Methods." *IEEE Transactions on Geoscience and Remote Sensing* 43 (10): 2376–2385. doi:10.1109/TGRS.2005.856106.

Padwick, C., M. Deskevich, F. Pacifici, and S. Smallwood. 2010. "WorldView-2 Pan-sharpening." ASPRS 2010 Annual Conference, San Diego, CA, USA, vol. 2630.

Pohl, C., and J. van Genderen. 2016. *Remote Sensing Image Fusion: A Practical Guide*. Boca Raton, FL: CRC Press.

Pohl, C., and J. L. Van Genderen. 1998. "Review Article Multisensor Image Fusion in Remote Sensing: Concepts, Methods and Applications." *International Journal of Remote Sensing* 19 (5): 823–854. doi:10.1080/014311698215748.

Ranchin, T., and L. Wald. 2000. "Fusion of High Spatial and Spectral Resolution Images: The ARSIS Concept and Its Implementation." *Photogrammetric Engineering & Remote Sensing* 66: 49–61.

Siddiqui, Y. 2003. "The Modified IHS Method for Fusing Satellite Imagery." ASPRS 2003 Annual Conference, Anchorage, Alaska.

Strait, M., S. Rahmani, and D. Markurjev. 2008. "Evaluation of Pan-Sharpening Methods." UCLA Department of Mathematics.

Sun, W., B. Chen, and D. Messinger. 2014. "Nearest-neighbor Diffusion-based Pan-sharpening Algorithm for Spectral Images." *Optical Engineering* 53: 1. doi:10.1117/1.OE.53.1.013107.

Tran, D. H., M. Y. Cheng, and D. Prayogo. 2016. "A Novel Multiple Objective Symbiotic Organisms Search (MOSOS) for Time–Cost–Labor Utilization Tradeoff Problem." *Knowledge-Based Systems* 94: 132–145. doi:10.1016/j.knosys.2015.11.016.

Vivone, G., R. Restaino, M. Dalla Mura, G. Licciardi, and J. Chanussot. 2014. "Contrast and Error-based Fusion Schemes for Multispectral Image Pansharpening." *IEEE Geoscience and Remote Sensing Letters* 11 (5): 930–934. doi:10.1109/LGRS.2013.2281996.

Wald, L. 2000. "Quality of High Resolution Synthesized Images: Is There a Simple Criterion?" 3rd Conference Fusion of Earth data: merging point measurements, raster maps and remotely sensed images, Sophia Antipolis, France, pp. 99–103.

Wald, L., and T. Ranchin. 2002. "Liu'Smoothing Filter-based Intensity Modulation: A Spectral Preserve Image Fusion Technique for Improving Spatial Details." *International Journal of Remote Sensing* 23: 593–597. doi:10.1080/01431160110088772.

Wald, L., T. Ranchin, and M. Mangolini. 1997. "Fusion of Satellite Images of Different Spatial Resolutions: Assessing the Quality of Resulting Images." *Photogrammetric Engineering & Remote Sensing* 63: 691–699.

Wang, Z., and A. C. Bovik. 2002. "A Universal Image Quality Index." *IEEE Signal Processing Letters* 9 (3): 81–84. doi:10.1109/97.995823.

Wang, Z., A. C. Bovik, H. R. Sheikh, and E. P. Simoncelli. 2004. "Image Quality Assessment: From Error Visibility to Structural Similarity." *IEEE Transactions on Image Processing* 13 (4): 600–612. doi:10.1109/TIP.2003.819861.

Wang, Z., and Q. Li. 2011. "Information Content Weighting for Perceptual Image Quality Assessment." *IEEE Transactions on Image Processing* 20 (5): 1185–1198. doi:10.1109/TIP.2010.2092435.

Wang, Z., E. P. Simoncelli, and A. C. Bovik, 2003. "Multi-scale Structural Similarity for Image Quality Assessment," 37th Asilomar Conference on Signals, Systems & Computers, Pacific Grove, CA, 2: pp. 1398–1402. doi: 10.1109/ACSSC.2003.1292216.

Yilmaz, V., and O. Gungor. 2016a. "Fusion of Very High-resolution UAV Images with Criteria-based Image Fusion Algorithm." *Arabian Journal of Geosciences* 9 (1): 59. doi:10.1007/s12517-015-2109-8.

Yilmaz, V., and O. Gungor. 2016b. "Determining the Optimum Image Fusion Method for Better Interpretation of the Surface of the Earth." *Norsk Geografisk Tidsskrift-Norwegian Journal of Geography* 70 (2): 69–81. doi:10.1080/00291951.2015.1126761.

Yilmaz, V., C. Serifoglu Yilmaz, and O. Gungor. 2019. "Genetic Algorithm-Based Synthetic Variable Ratio Image Fusion." *Geocarto International (Just-accepted)* 1–17. doi:10.1080/10106049.2019.1629649.

Zeng, Y., W. Huang, M. Liu, H. Zhang, and B. Zou. 2010. "Fusion of Satellite Images in Urban Area: Assessing the Quality of Resulting Images." 18th IEEE International Conference on Geoinformatics, Beijing, China, pp. 1–4.

Zhang, Y. 1999. "A New Merging Method and Its Spectral and Spatial Effects." *International Journal of Remote Sensing* 20 (10): 2003–2014. doi:10.1080/014311699212317.

Zhang, Y. 2004. "Understanding Image Fusion." *Photogrammetric Engineering & Remote Sensing* 70 (6): 657–661.

Zhang, Y., and G. Hong. 2005. "An IHS and Wavelet Integrated Approach to Improve Pan-sharpening Visual Quality of Natural Colour IKONOS and QuickBird Images." *Information Fusion* 6 (3): 225–234. doi:10.1016/j.inffus.2004.06.009.

Zhou, J., D. L. Civco, and J. A. Silander. 1998. "A Wavelet Transform Method to Merge Landsat TM and SPOT Panchromatic Data." *International Journal of Remote Sensing* 19 (4): 743–757. doi:10.1080/014311698215973.